

One Pass Is Not Enough: Recursive Latent Refinement for Generative Models

Mehdi Esmaeilzadeh¹ Alexia Jolicoeur-Martineau² Chirag Vashist¹ Ke Li¹

¹Simon Fraser University ²Independent



Figure 1: Unconditional AFHQ-v1 (512×512) samples from StyleGAN2-ADA without RTM (left) vs. with RTM (right). RTM improves both quality (FID 4.79 vs. 4.99) and diversity (Recall 0.565 vs. 0.507).

Abstract

Despite remarkable progress, image generation is far from solved. The dominant metric, FID, conflates sample fidelity with mode coverage and is close to being saturated. Yet a model can still exhibit mode collapse while achieving a low FID, since a handful of sharp, near-duplicate images can outscore a model that faithfully covers the full data distribution. We argue that precision and recall are essential complements to FID, and that because FID is already saturated, the more meaningful goal is to improve diversity and coverage. Achieving high recall requires a model that explicitly prioritizes mode coverage, unlike most generative models, which optimize sample fidelity. We introduce RTM, which replaces the single-pass latent mapping in style-based generators with an iterative refinement process, and show that this consistently improves both quality and diversity. Integrated with Implicit Maximum Likelihood Estimation (IMLE), which optimizes mode coverage by design, RTM achieves the highest precision and recall among current state-of-the-art approaches while maintaining competitive FID, with improvements across CIFAR-10, CelebA-HQ at 256×256 , and nine few-shot benchmarks. RTM also improves StyleGAN2 and StyleGAN2-ADA on CIFAR-10 and AFHQ-v1 at 512×512 , demonstrating that the benefit is not specific to IMLE. Unlike flow-matching baselines that achieve competitive FID at the expense of coverage, recursive refinement improves both quality and diversity simultaneously.

1 Introduction

Research on generative models has made remarkable advances and produced a rich family of methods, including diffusion models [Ho et al., 2020, Karras et al., 2022], flow matching [Lipman et al., 2023, Liu et al., 2022a], and generative adversarial networks (GANs) [Goodfellow et al., 2014, Karras et al., 2020b]. On image generation tasks, Fréchet inception distance (FID) [Heusel et al., 2017] has become the standard evaluation metric, and with each successive paper, the state-of-the-art FID has fallen to the low single digits and is close to being saturated. Does this mean that image generation is now solved?

We argue that image generation is still far from being solved, and the remarkable progress in improving FID has obscured other important challenges. A well-documented limitation of FID [Kynkäänniemi et al., 2019, Naeem et al., 2020] is that it conflates sample fidelity with mode coverage into a single scalar, making it impossible to distinguish a model that generates realistic but low-diversity samples from one that faithfully covers the full data distribution.

A model that produces a handful of sharp, near-duplicate images per class can therefore attain a lower FID than one that faithfully covers the long tail. In other words, a model can attain a low FID even if it exhibits *mode collapse*, which is a long-standing problem with generative models where they concentrate on a few high-fidelity modes and drop others [Salimans et al., 2016, Lucic et al., 2018, Arora et al., 2017, Goodfellow, 2016]. Distilled and few-step diffusion models show a similar erosion in the number of modes covered as their step count shrinks [Salimans and Ho, 2022, Yin et al., 2024, Schwag et al., 2022].

Precision and Recall [Kynkäänniemi et al., 2019, Naeem et al., 2020] directly address this by measuring fidelity and coverage independently. Precision measures the fraction of generated samples that are realistic, and Recall measures the fraction of the real data distribution that the generator covers. Unlike FID, where mode collapse can be masked by sharp, concentrated samples, a drop in Recall makes coverage failure immediately visible.

This view informs our goal and choice of methodology. Because FID is already close to being saturated, our goal is not necessarily to push FID even lower. Instead, we aim to improve Precision and Recall, while still maintaining a reasonably low FID. Improving Recall in particular requires a training objective that explicitly targets mode coverage; most generative models optimize sample fidelity instead. Our method is based on Implicit Maximum Likelihood Estimation (IMLE), which satisfies this requirement by construction: it guarantees every training image a nearby generated sample, making mode collapse impossible by design. RTM-IMLE achieves the highest Precision and Recall among current state-of-the-art approaches while maintaining competitive FID. Figure 2 places IMLE in the broader landscape of generative models along the quality, diversity, and speed axes.

IMLE works by minimizing the distance between each data samples to its nearest generated sample, where the nearness may be defined in raw data space or latent space. It resists mode collapse by construction, since every training image is guaranteed a nearby generated image, but it has historically lagged behind in sample quality. Sample quality is limited not only by the training objective but also by the generator’s architecture responsible for mapping noise to images. IMLE-based methods have generally relied on the StyleGAN family of architectures for their generators [Li and Malik, 2018, Aghabozorgi et al., 2023, Vashist et al., 2024]. The StyleGAN architecture [Karras et al., 2019, 2020b,a] consists of a small mapping network that turns Gaussian noise $z \in \mathbb{R}^d$ into a style code $w \in \mathbb{R}^d$, and a convolutional decoder that conditions on w via Adaptive Instance Normalization [Huang and Belongie, 2017] to progressively upsamples a learned constant feature map into an image. The mapping network is a multilayer perceptron (MLP) network (generally with 8 layers) processed in a single forward pass.

In every prior IMLE and StyleGAN model, the mapping network is a plain MLP processed in a single forward pass [Karras et al., 2019, 2020b]. This forces the mapper to determine every aspect of the style code simultaneously, identity, structure, texture, and fine detail, in one shot. Because the decoder is highly sensitive to small variations in w [Karras et al., 2019], any inaccuracy in w at this stage produces visible artifacts in the final image. A natural response is to make the MLP deeper or wider, but this does not change the fundamental structure: a feed-forward chain still determines w in a single pass, with no mechanism to revise an earlier decision in light of later computation. Our central insight is that refinement constitutes a qualitatively different computation: the mapper produces a coarse estimate of w first and progressively corrects it over multiple cycles, with early

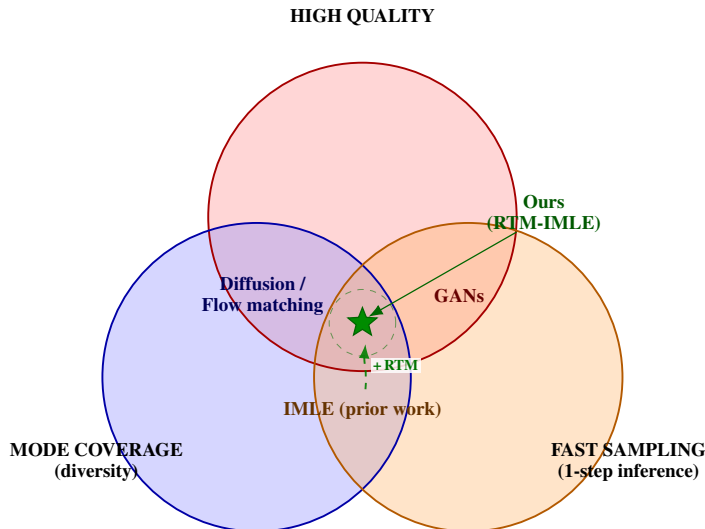


Figure 2: Each circle marks one of quality, diversity, or fast (1-step) sampling; families sit at the intersections. RTM-IMLE pushes IMLE into the triple intersection. Adapted from Xiao et al. [2022].

cycles establishing coarse structure such as identity, composition, and pose, and later cycles refining texture, sharpening, and color.

To this end, we propose the Recursive Token Mapper (RTM), a drop-in replacement for the single-pass MLP in the StyleGAN architecture. RTM adapts the Tiny Recursive Model of Jolicoeur-Martineau [2025] to the generative setting, refining latent tokens through nested recursive cycles to gain effective depth through recursion rather than width; the full architecture is described in Section 3.2.

In summary, our contributions are: **(i)** the Recursive Token Mapper, a drop-in recursive replacement for the MLP mapping network shared by the StyleGAN family of generators; **(ii)** integrated with RS-IMLE [Vashist et al., 2024], RTM improves FID, precision, and recall over a vanilla RS-IMLE baseline on nine few-shot benchmarks, unconditional CIFAR-10, and CelebA-HQ at 256×256 , while retaining IMLE’s direct latent-to-image map and one-step generation; and **(iii)** integrated with the adversarially-trained StyleGAN2 [Karras et al., 2020b] and StyleGAN2-ADA [Karras et al., 2020a] generators, RTM lowers FID and raises precision, density, and coverage on unconditional CIFAR-10 and AFHQ-v1 relative to the corresponding non-recursive baselines, showing that the benefit is not confined to the context of IMLE training.

2 Related Work

2.1 Diffusion and flow-matching

The strongest current baselines in terms of FID belong to the diffusion and flow-matching families: DDPM [Ho et al., 2020], EDM [Karras et al., 2022], LSGM [Vahdat et al., 2021], Flow Matching (FM) [Lipman et al., 2023], OT Flow Matching [Tong et al., 2024], Mean Flows [Geng et al., 2025], and Inductive Moment Matching [Zhou et al., 2025]. These methods learn a time-dependent vector field $u_\theta(x, t)$ that defines an ordinary or stochastic differential equation taking Gaussian noise at $t=0$ to a data sample at $t=1$.

Generation from a noise code z is therefore not a function $G_\theta(z)$, but the trajectory of an iterative solver initialised at z , which has three consequences. First, the correspondence between a noise code and an image is only defined implicitly through the solver; the training objective does not pull a particular latent towards a specific training image, but matches expected vector fields. Second, reaching a low-FID sample typically requires tens to hundreds of neural function evaluations; distilled one-step variants [Salimans and Ho, 2022, Yin et al., 2024, Song et al., 2023, Geng et al., 2025, Zhou et al., 2025] accelerate inference but consistently trade away coverage in the process: Yin et al. [2024] explicitly observe a drop in sample diversity when collapsing a multi-step diffusion teacher

into a single-step student, and Salimans and Ho [2022] report a similar quality–diversity erosion as the number of sampling steps shrinks. Third, even at full step count diffusion solvers systematically under-cover low-density regions of the data distribution [Sehwag et al., 2022].

2.2 Generative adversarial networks

GANs [Goodfellow et al., 2014, Karras et al., 2019, 2020b,a, Sauer et al., 2022] sit at the opposite end of the same trade-off: they generate in a single forward pass, but a long line of work, starting with Salimans et al. [2016], Goodfellow [2016], Arora et al. [2017] and quantified at scale by Lucic et al. [2018], has established that adversarial training is prone to mode collapse, where the generator concentrates on a few high-fidelity modes and silently drops others. Considerable effort has gone into mitigating this failure mode, including training stabilizers and regularisers [Salimans et al., 2016, Karras et al., 2020b], data augmentation strategies [Karras et al., 2020a], and hybrid GAN/diffusion objectives [Xiao et al., 2022], but the failure mode remains the central concern with adversarial training. Style-based GAN families [Karras et al., 2019, 2020b,a] introduced the two-component design of a mapping network followed by a convolutional decoder that our RTM builds on.

2.3 IMLE-family generators

Implicit Maximum Likelihood Estimation (IMLE) [Li and Malik, 2018] is a direct-mapping alternative that trains a generator $G_\theta(z)$ with the explicit guarantee that every training image x_i has some latent z_i whose generated image $G_\theta(z_i)$ is close to it in a learned feature space. A pool of random latents is sampled, and the nearest generated sample to each x_i is selected, and the generator is pulled towards the matched training image. This one-to-one assignment is what makes IMLE robust to the mode-collapse failure modes documented for adversarial [Lucic et al., 2018] and distilled-diffusion [Yin et al., 2024, Salimans and Ho, 2022] generators: every real image is guaranteed a nearby preimage by construction. Inference is a single forward pass, and the latent-to-image map is an ordinary neural network. Adaptive IMLE (AdaIMLE) [Aghabozorgi et al., 2023] introduced adaptive per-image thresholds during training, and the more recent Rejection-Sampling IMLE (RS-IMLE) [Vashist et al., 2024] closes the train and test prior gap by rejecting pool latents whose generated images are too close to existing training images. Across this entire line of work, the mapping network has remained an eight-layer MLP inherited from StyleGAN.

2.4 Recursive and iterative architectures

Recursive computation has a long history in deep learning, from RNN-style weight-tying to Universal Transformers [Dehghani et al., 2019] and recent looped-transformer analyses [Giannou et al., 2023]. Closer to our setting, the Hierarchical Reasoning Model (HRM) [Wang et al., 2025] and its compact successor, the Tiny Recursive Model (TRM) [Jolicoeur-Martineau, 2025] introduce nested $H \times L$ recursive cycles around a single shared block, paired with deep supervision and a learned halting head, on discrete reasoning benchmarks. We adapt this recursive architecture to the generative setting as a mapping network for image generation.

3 Method

3.1 Background: IMLE and RS-IMLE

IMLE [Li and Malik, 2018] trains a generator G_θ on a dataset $\{x_1, \dots, x_n\}$ by guaranteeing that every training image is paired with a noise vector that maps near it. At each round, a pool of $m \gg n$ candidate latents $\{\tilde{z}_j\}_{j=1}^m$ is drawn from a Gaussian prior $p(z)$, decoded into images $G_\theta(\tilde{z}_j)$, and matched to training images by a nearest-neighbour search in a learned feature space ϕ . The matched latents are then used as training inputs:

$$\sigma(i) = \arg \min_{j \in \{1, \dots, m\}} \|\phi(x_i) - \phi(G_\theta(\tilde{z}_j))\|_2, \quad \min_{\theta} \sum_{i=1}^n \mathcal{L}(G_\theta(\tilde{z}_{\sigma(i)}), x_i), \quad (1)$$

where \mathcal{L} combines an LPIPS [Zhang et al., 2018] perceptual term and a pixel-level reconstruction term. Pairing every training image with its own latent makes mode collapse impossible by construction, and inference is a single forward pass.

RS-IMLE [Vashist et al., 2024] closes the gap between the matched-latent training distribution and the i.i.d. Gaussian inference distribution by rejecting any pool sample whose generated image is closer than a threshold ε to some training image, so the generator only learns from latents that look like genuine prior draws.

3.2 Improved mapping network: the Recursive Token Mapper (RTM)

Following StyleGAN [Karras et al., 2019], the IMLE generator factors into two components. A small mapping network maps a noise vector $z \sim \mathcal{N}(0, I_d)$ to a style vector $w \in \mathbb{R}^d$, and a convolutional decoder conditions on w via Adaptive Instance Normalization [Huang and Belongie, 2017] and progressively upsamples a learned constant feature map into an image. The decoder architecture follows each baseline: residual blocks with 1×1 and 3×3 convolutions, GELU activations and noise injection for the few-shot runs; ConvNeXt-style blocks [Liu et al., 2022b] for CIFAR-10 at 32×32 and CelebA-HQ at 256×256 ; and the StyleGAN2 / StyleGAN2-ADA [Karras et al., 2020b,a] convolutional decoder for the adversarial-training experiments.

The mapping network is the single component we change. In all prior IMLE work, and in the StyleGAN family the architecture is borrowed from, this network is an MLP processed in a single forward pass: eight layers in the RS-IMLE experiments and two layers in the StyleGAN2 experiments. The decoder is highly sensitive to small variations in w , so the mapper’s placement of w is a sample-quality bottleneck. We replace it with the Recursive Token Mapper (RTM) introduced in the next subsection, which adapts the Tiny Recursive Model of Jolicoeur-Martineau [2025] to the generative setting.

RTM produces the same style vector $w \in \mathbb{R}^d$ from the same noise vector $z \in \mathbb{R}^d$ as the MLP mapper it replaces, but it does so by repeatedly applying a single small block f to a refined latent representation rather than passing z through a deep stack of independent layers. The depth of computation is controlled by two integers: L inner cycles and H refinement steps. Because f is reused at every iteration, increasing either count increases the effective depth of the mapper without adding parameters. Following Jolicoeur-Martineau [2025], the two-level structure separates a fast-adapting inner state Z_L (updated L times per step) from a slower-accumulating outer state Z_H (updated once per step), while re-injecting Z_0 at every inner cycle keeps the recursion anchored to the original noise.

Recursive H/L cycles. After PixelNorm, z is linearly lifted into a sequence of latent tokens Z_0 , which seeds two states: an inner state Z_L and an outer state Z_H , both initialized from fixed vectors. Within one step, Z_L is updated L times by f conditioned on the current outer state and on Z_0 ; the refreshed Z_L then drives a single update of Z_H by f . This is repeated for H steps in total, re-injecting Z_0 at every inner cycle so the recursion never loses contact with the original noise. The final Z_H is read out by a linear layer to produce w . Algorithm 1 in the appendix gives the full step-by-step pseudo-code, including the projection and readout layers.

Choice of block. The shared block f enables information exchange between latent tokens and is otherwise unconstrained. We use the MLP-Mixer-style token-mixing block of Tolstikhin et al. [2021] throughout this work: layer normalization, a SwiGLU MLP along the sequence axis to mix tokens, and a second SwiGLU MLP along the channel axis. This avoids the quadratic cost of attention while still permitting cross-token communication. To validate this design choice, we also ran the original TRM block of Jolicoeur-Martineau [2025], which replaces token mixing with multi-head self-attention on the token grid, on the few-shot benchmarks (Section D). The MLP-Mixer variant was consistently better in FID and noticeably faster per step, and its advantage in both quality and wall-clock grows with sequence length and dataset size; we therefore use MLP-Mixer for all of the larger CIFAR-10, CelebA-HQ, AFHQ-v1, and StyleGAN runs.

Short-gradient optimization. Recursing through H steps would otherwise multiply the activation memory of the mapper by H , since the full computation graph of every step would need to be retained for backpropagation. To keep training memory tractable, only the final step is differentiated through; all earlier steps run without tracking gradients, so their intermediate activations are immediately discarded. This preserves the representational benefit of deep recursion while keeping the per-step training memory cost close to that of a single feed-forward block, analogous to truncated backpropagation through time.

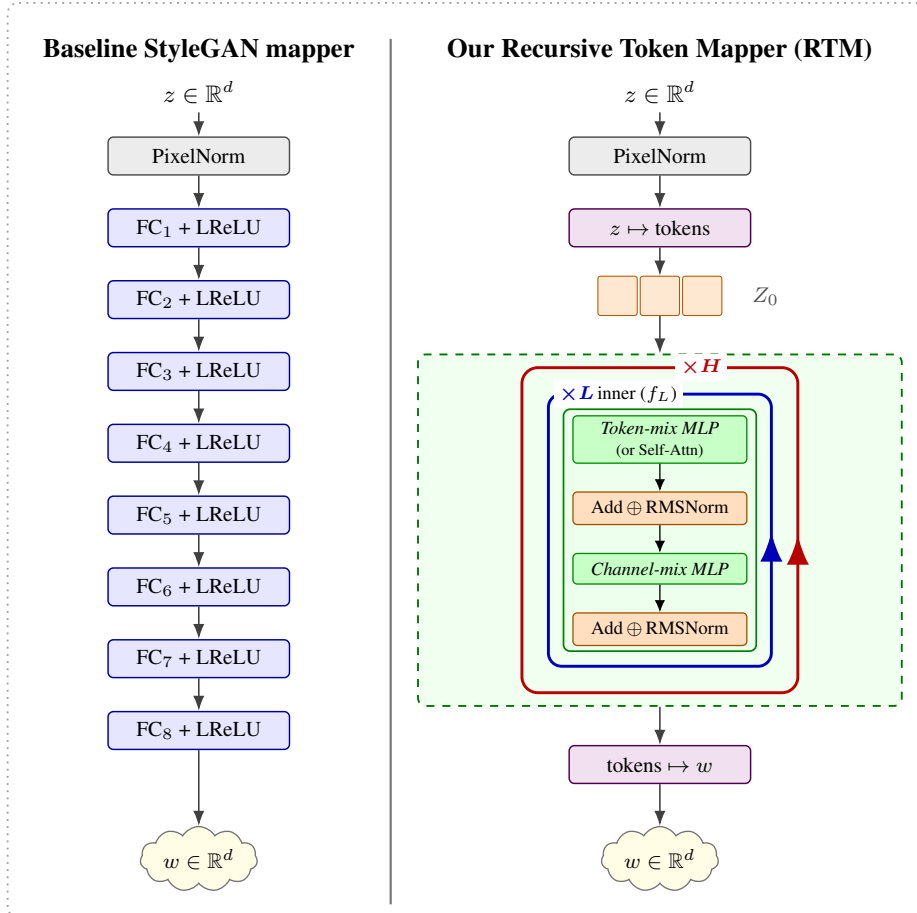


Figure 3: StyleGAN mapper [Karras et al., 2019] (left) vs. our RTM (right): a shared block iterated L times (blue) repeated for H refinement steps (red). The IMLE loss is applied only to the final style w ; no supervision is applied between refinement steps.

4 Experiments

Experimental setup. We evaluate RTM in two training regimes. In the IMLE regime (Sections 4.1–4.2), we integrate RTM as the mapping network of RS-IMLE and evaluate on unconditional CIFAR-10 at 32×32 and unconditional CelebA-HQ at 256×256 . In the adversarial regime (Section 4.3), we integrate RTM as the mapping network of StyleGAN2 and StyleGAN2-ADA and evaluate on unconditional CIFAR-10 at 32×32 and unconditional AFHQ-v1 at 512×512 . Results on nine standard few-shot benchmarks are deferred to Appendix D. The decoder, regularizer, optimizer, and training schedule are identical between baseline and RTM runs in every comparison; only the mapping network changes. Per-dataset hyperparameters are in Appendix F.

Evaluation. We use FID [Heusel et al., 2017], Inception Score [Salimans et al., 2016], and the $k=3$ nearest-neighbour Precision and Recall of Kynkäänniemi et al. [2019] for a comprehensive evaluation; for the StyleGAN runs we additionally report Density and Coverage [Naeem et al., 2020]. FID measures the distance between Inception-v3 features of generated and real images; IS and Precision measure sample fidelity, Recall measures diversity, and Density and Coverage are kNN-based refinements of Precision and Recall. We compute all four metrics from the same Inception-v3 activations of 50,000, 30,000, and 5,000 generated samples for CIFAR-10, CelebA-HQ, and the few-shot benchmarks respectively, with the corresponding training set as the reference; for AFHQ-v1 we use the 14,630-image test split as the reference. Every reproduced row in our tables is evaluated by us from the corresponding method’s official released checkpoint, so that all rows in a given table are comparable; rows marked with † are taken from the original publication.

Table 1: Unconditional CIFAR-10 (32×32 , 50,000 samples). Time / image is the wall-clock per generated image at batched inference on a single H100 (lower is faster); see App. H for the protocol. **Bold/underline**: best/second-best per metric column. † taken from the original publication.

Method	Precision \uparrow	Recall \uparrow	IS \uparrow	FID \downarrow	Time (ms) \downarrow
<i>GAN family (1-NFE, adversarial)</i>					
StyleGAN2 [†] [Karras et al., 2020a]	–	–	9.21	8.32	–
StyleGAN-XL [Sauer et al., 2022]	0.674	0.467	–	1.86	3.6
<i>Diffusion / score-based / consistency family (multi-NFE unless noted)</i>					
DDPM [Ho et al., 2020]	0.619	0.567	8.62	11.18	13.3
NVAE+VAEBM [†] [Xiao et al., 2021]	–	–	8.43	12.19	–
LSGM [Vahdat et al., 2021]	0.703	0.596	10.07	2.79	570
ProxDM (hybrid) [Fang et al., 2025]	0.658	0.570	8.98	4.55	185
RGM (KLD-D, 4 steps) [Choi et al., 2023]	0.653	0.526	9.28	4.85	1.4
EDM [Karras et al., 2022]	0.675	0.618	9.91	<u>1.96</u>	14.6
Consistency Models (CD, 1-NFE) [Song et al., 2023]	0.688	0.560	9.72	<u>3.57</u>	1.8
Consistency Models (CT, 1-NFE) [Song et al., 2023]	0.702	0.419	8.61	8.79	1.5
<i>Flow-matching family (multi-NFE, no direct latent-to-image map)</i>					
Flow Matching [Lipman et al., 2023]	0.651	0.589	9.28	3.72	23.8
OT-CFM [Tong et al., 2024]	0.652	0.592	9.25	3.68	21.1
Mean Flows ($N=1$) [Geng et al., 2025]	0.687	0.586	<u>10.10</u>	2.87	1.3
Mean Flows ($N=2$) [Geng et al., 2025]	0.704	0.582	10.13	2.83	1.8
Inductive Moment Matching ($N=1$) [Zhou et al., 2025]	0.659	0.593	<u>10.10</u>	3.16	1.3
Inductive Moment Matching ($N=2$) [Zhou et al., 2025]	0.674	0.615	10.08	2.01	1.7
<i>IMLE family (1-NFE, direct latent-to-image map)</i>					
RS-IMLE Baseline	<u>0.853</u>	<u>0.738</u>	10.00	5.69	6.4
RS-IMLE + RTM ($H=16, L=1$) (Ours)	0.896	0.773	10.08	3.97	6.7

4.1 Unconditional CIFAR-10

Setup. We evaluate on CIFAR-10 [Krizhevsky, 2009] at 32×32 . The matched comparison is RS-IMLE with the same decoder; Table 1 additionally covers representative GAN, diffusion / score-based / consistency, and flow-matching baselines (citations in the table).

Results. Within the IMLE family, RTM lowers FID by 30% over the matched RS-IMLE baseline while simultaneously improving Precision, Recall, and IS. Across families, RTM closes most of the remaining FID gap to the strongest diffusion and flow-matching baselines while retaining IMLE’s one-step inference. The defining feature of our method is its position on the Precision/Recall axes: RTM achieves the highest Precision and the highest Recall of any method in Table 1, despite being trained without an adversary or a diffusion solver. By contrast, flow-matching methods such as Mean Flows achieve a lower FID (2.83) but substantially lower Precision (0.704) and Recall (0.582), a pattern consistent with mode collapse: concentrating on high-density modes can improve FID while leaving large portions of the data distribution uncovered. This illustrates precisely why FID alone is an insufficient criterion for evaluating generative models.

4.2 Unconditional CelebA-HQ at 256×256

Setup. CelebA-HQ [Karras et al., 2018] at 256×256 , same RS-IMLE pipeline and decoder as described in Appendix C; only the mapping network changes. We compare against the matched RS-IMLE baseline and the strongest publicly-checkpointed unconditional CelebA-HQ generators (DDPM, DDGAN, RDM, StyleSwin); citations are in Table 2. NVAE and VAEBM rows are taken verbatim from Vahdat et al. [2021].

Results. Within the IMLE family, RTM cuts FID by 27% over the matched RS-IMLE baseline while simultaneously improving Precision, Recall, and IS. RDM is the strongest non-IMLE method by FID, but RTM achieves both the highest Precision and the highest Recall in the table while generating each sample in a single feed-forward pass rather than a multi-step diffusion solver. The

Table 2: Unconditional CelebA-HQ (256×256, 30,000 samples). Time / image as in Table 1 (single H100, batched). **Bold/underline**: best/second-best per metric column. Rows without † are our evaluations of each method’s released checkpoint. RS-IMLE + RTM uses the ($H=16, L=2$) configuration.

Method	Precision ↑	Recall ↑	IS ↑	FID ↓	Time (ms) ↓
<i>VAE / score-based family</i>					
NVAE† [Vahdat and Kautz, 2020]	–	–	–	29.76	–
VAEBM† [Xiao et al., 2021]	–	–	–	20.38	–
LSGM [Vahdat et al., 2021]	0.761	0.337	2.61	11.69	1,070
<i>Diffusion / score-based family</i>					
DDPM [Ho et al., 2020]	0.447	0.147	2.44	33.49	577
DDGAN [Xiao et al., 2022]	0.683	0.205	2.71	15.83	8.8
ProxDM (hybrid) [Fang et al., 2025]	0.634	0.217	2.76	19.94	365
RDM [Teng et al., 2024]	0.709	<u>0.495</u>	3.29	5.77	1,713
<i>GAN family</i>					
StyleSwin [Zhang et al., 2022]	0.626	0.362	3.46	<u>7.99</u>	39.6
<i>IMLE family (1-NFE, direct latent-to-image map)</i>					
RS-IMLE Baseline	<u>0.924</u>	0.491	3.18	15.43	18.1
RS-IMLE + RTM ($H=16, L=2$) (Ours)	0.952	0.592	<u>3.36</u>	10.67	19.6

Table 3: RTM as the StyleGAN2 / StyleGAN2-ADA mapper. Each (no RTM, +RTM) pair shares the same training pipeline; only the mapping network changes. Bold marks the better entry in each pair.

Dataset	Method	FID ↓	IS ↑	Prec. ↑	Rec. ↑	Dens. ↑	Cov. ↑
CIFAR-10 (32×32)	StyleGAN2 (no RTM)	3.88	10.20	0.734	0.664	0.987	0.894
	StyleGAN2 + RTM (Ours)	3.55	10.21	0.740	0.661	1.017	0.901
	StyleGAN2-ADA (no RTM)	2.31	10.46	0.744	0.685	1.050	0.932
	StyleGAN2-ADA + RTM (Ours)	2.31	10.50	0.754	0.669	1.063	0.933
AFHQ-v1 (512×512)	StyleGAN2-ADA (no RTM)	4.99	12.91	0.857	0.507	1.282	0.835
	StyleGAN2-ADA + RTM (Ours)	4.79	12.49	0.859	0.565	1.236	0.833

remaining FID gap mirrors the trade-off observed on CIFAR-10 (Table 1) and is the cost of insisting on a direct latent-to-image map.

4.3 RTM as the mapper of a StyleGAN2 generator

Setup. To test whether the benefit of recursive mapping is specific to IMLE training, we plug RTM into the mapping network of StyleGAN2 and StyleGAN2-ADA [Karras et al., 2020b,a] and train them with the reproductions of those recipes from Kang et al. [2021]. We evaluate two settings: unconditional CIFAR-10 at 32×32 with StyleGAN2 and StyleGAN2-ADA, and unconditional AFHQ-v1 at 512×512 with StyleGAN2-ADA. The decoder, regularizer, augmentation pipeline, optimizer, and training schedule are identical between baseline and RTM runs; only the two-layer MLP mapper is replaced by an RTM with (H, L)=(16, 1). All numbers in Table 3 are reported with the StudioGAN evaluation pipeline of Kang et al. [2021], using Improved Precision/Recall [Kynkäänniemi et al., 2019] and Density/Coverage [Naeem et al., 2020]; the FID and Precision/Recall implementations differ slightly in feature extractor, reference statistics, and image preprocessing from those used in Tables 1 and 2.

Results. On CIFAR-10 with StyleGAN2, RTM lowers FID from the StudioGAN-reported 3.88 to 3.55 and improves IS, Precision, Density, and Coverage; Recall is essentially unchanged. With ADA augmentation, the RTM-mapped chain matches the StudioGAN baseline’s FID of 2.31 while improving IS, Precision, Density, and Coverage. On AFHQ-v1 with StyleGAN2-ADA, RTM lowers FID from 4.99 to 4.79 and increases Recall from 0.507 to 0.565; the baseline retains a small edge on IS, Density, and Coverage. Because the only difference between the paired rows is the mapping

Table 4: Effect of varying the number of refinement steps H at inference for the trained ($H=16, L=1$) configuration. **Bold**: best per dataset.

Dataset	Inference-time H	FID ↓	IS ↑	Precision ↑	Recall ↑
CIFAR-10	$H=8$ (half of native)	4.04	10.07	0.896	0.774
	$H=16$ (native)	3.97	10.08	0.896	0.773
	$H=32$ (double)	3.94	10.09	0.897	0.775
	$H=64$ (quadruple)	3.94	10.08	0.895	0.774
CelebA-HQ	$H=8$ (half of native)	12.31	3.29	0.941	0.537
	$H=16$ (native)	12.22	3.30	0.940	0.541
	$H=32$ (double)	12.19	3.30	0.939	0.541
	$H=64$ (quadruple)	12.20	3.30	0.939	0.541

network, these gains show that the benefit of recursive mapping is not specific to IMLE training and transfers to an adversarial recipe.

4.4 Analysis

Varying the number of refinement steps at inference. Because the IMLE loss is applied only to the final style w and H acts as a computational hyperparameter (Section 3.2) rather than as a per-step training signal, the number of refinement steps used at inference can differ from the value used during training without any retraining or fine-tuning. After training the ($H=16, L=1$) configuration on CIFAR-10 and CelebA-HQ, we re-evaluate the trained model at $H \in \{8, 16, 32, 64\}$, leaving every other component of the architecture and evaluation pipeline unchanged.

On both datasets, FID improves modestly as H increases from the trained value of 16 up to 32 and then plateaus at $H=64$, while Precision and Recall remain essentially constant across the entire sweep. A single trained model can therefore exchange a small amount of additional inference compute for a slight improvement in fidelity, or, conversely, halve its inference cost with only a marginal increase in FID, in either case without any retraining or fine-tuning.

5 Conclusion

Generative models are best evaluated with FID alongside Precision and Recall, since FID alone conflates fidelity with mode coverage and rewards sharp but low-diversity samples. Within that evaluation frame, we introduced the Recursive Token Mapper (RTM), a drop-in replacement for the single-pass MLP mapping network used by style-based generators. RTM is the first method leveraging TRM for continuous image generation ([Baek et al., 2026] first applied a generative TRM to binary black-and-white pictures). RTM gains effective depth through recursion rather than width, preserving IMLE’s one-step inference. It consistently improves FID, Precision, and Recall across nine few-shot benchmarks, CIFAR-10, and CelebA-HQ, and also improves StyleGAN2 and StyleGAN2-ADA, demonstrating that the benefit is not specific to IMLE.

Limitations. Our experiments are limited to the few-shot benchmarks, CIFAR-10, CelebA-HQ, and AFHQ-v1; we do not report on ImageNet, as IMLE’s per-step cost (nearest-neighbour search) scales with dataset size, making ImageNet training infeasible within our compute budget. We leave large-scale IMLE to future work.

Broader Impact. Better coverage of real data distributions benefits data augmentation and scientific image synthesis, and one-step inference improves accessibility. Improved generators could facilitate disinformation or deepfakes, though our incremental architectural change on standard benchmarks at modest resolutions limits direct misuse potential relative to large-scale systems already in deployment.

Future work. HRM and TRM [Wang et al., 2025, Jolicoeur-Martineau, 2025] pair their recursive core with a learned halting head that allocates more compute to hard inputs and less to easy ones. A natural next step is a halting signal compatible with IMLE, so RTM can focus on hard latents (rare modes) without hand-picking H at inference.

References

- Mehran Aghabozorgi, Shichong Peng, and Ke Li. Adaptive IMLE for few-shot pretraining-free generative modelling. In *International Conference on Machine Learning*, 2023.
- Sanjeev Arora, Rong Ge, Yingyu Liang, Tengyu Ma, and Yi Zhang. Generalization and equilibrium in generative adversarial nets (GANs). In *International Conference on Machine Learning*, 2017.
- Junyeob Baek, Mingyu Jo, Minsu Kim, Yoshua Bengio, and Sungjin Ahn. Generative recursive reasoning models. *ICLR 2026 Workshop on AI with Recursive Self-Improvement*, 2026.
- Jaemoo Choi, Yesom Park, and Myungjoo Kang. Restoration based generative models. In *International Conference on Machine Learning*, 2023.
- Yunjey Choi, Youngjung Uh, Jaejun Yoo, and Jung-Woo Ha. StarGAN v2: Diverse image synthesis for multiple domains. In *Conference on Computer Vision and Pattern Recognition*, 2020.
- Mostafa Dehghani, Stephan Gouws, Oriol Vinyals, Jakob Uszkoreit, and Łukasz Kaiser. Universal transformers. In *International Conference on Learning Representations*, 2019.
- Zhengan Fang, Mateo Diaz Diaz, Sam Buchanan, and Jeremias Sulam. Beyond scores: Proximal diffusion models. In *Advances in Neural Information Processing Systems*, 2025.
- Zhengyang Geng, Mingyang Deng, Xingjian Bai, J. Zico Kolter, and Kaiming He. Mean flows for one-step generative modeling. *arXiv preprint arXiv:2505.13447*, 2025.
- Angeliki Giannou, Shashank Rajput, Jy-yong Sohn, Kangwook Lee, Jason D. Lee, and Dimitris Papailiopoulos. Looped transformers as programmable computers. In *International Conference on Machine Learning*, 2023.
- Ian Goodfellow. NIPS 2016 tutorial: Generative adversarial networks. *arXiv preprint arXiv:1701.00160*, 2016.
- Ian Goodfellow, Jean Pouget-Abadie, Mehdi Mirza, Bing Xu, David Warde-Farley, Sherjil Ozair, Aaron Courville, and Yoshua Bengio. Generative adversarial nets. In *Advances in Neural Information Processing Systems*, 2014.
- Martin Heusel, Hubert Ramsauer, Thomas Unterthiner, Bernhard Nessler, and Sepp Hochreiter. GANs trained by a two time-scale update rule converge to a local nash equilibrium. In *Advances in Neural Information Processing Systems*, 2017.
- Jonathan Ho, Ajay Jain, and Pieter Abbeel. Denoising diffusion probabilistic models. In *Advances in Neural Information Processing Systems*, 2020.
- Xun Huang and Serge Belongie. Arbitrary style transfer in real-time with adaptive instance normalization. In *International Conference on Computer Vision*, 2017.
- Alexia Jolicoeur-Martineau. Less is more: Recursive reasoning with tiny networks. *arXiv preprint arXiv:2510.04871*, 2025.
- Minguk Kang, Woohyeon Shim, Minsu Cho, and Jaesik Park. Rebooting ACGAN: Auxiliary classifier GANs with stable training. In *Advances in Neural Information Processing Systems*, 2021.
- Tero Karras, Timo Aila, Samuli Laine, and Jaakko Lehtinen. Progressive growing of GANs for improved quality, stability, and variation. In *International Conference on Learning Representations*, 2018.
- Tero Karras, Samuli Laine, and Timo Aila. A style-based generator architecture for generative adversarial networks. In *Conference on Computer Vision and Pattern Recognition*, 2019.
- Tero Karras, Miika Aittala, Janne Hellsten, Samuli Laine, Jaakko Lehtinen, and Timo Aila. Training generative adversarial networks with limited data. In *Advances in Neural Information Processing Systems*, 2020a.

- Tero Karras, Samuli Laine, Miika Aittala, Janne Hellsten, Jaakko Lehtinen, and Timo Aila. Analyzing and improving the image quality of StyleGAN. In *Conference on Computer Vision and Pattern Recognition*, 2020b.
- Tero Karras, Miika Aittala, Timo Aila, and Samuli Laine. Elucidating the design space of diffusion-based generative models. In *Advances in Neural Information Processing Systems*, 2022.
- Alex Krizhevsky. Learning multiple layers of features from tiny images. Technical report, University of Toronto, 2009.
- Tuomas Kynkäänniemi, Tero Karras, Samuli Laine, Jaakko Lehtinen, and Timo Aila. Improved precision and recall metric for assessing generative models. In *Advances in Neural Information Processing Systems*, 2019.
- Ke Li and Jitendra Malik. Implicit maximum likelihood estimation. *arXiv preprint arXiv:1809.09087*, 2018.
- Yaron Lipman, Ricky T. Q. Chen, Heli Ben-Hamu, Maximilian Nickel, and Matt Le. Flow matching for generative modeling. In *International Conference on Learning Representations*, 2023.
- Bingchen Liu, Yizhe Zhu, Kunpeng Song, and Ahmed Elgammal. Towards faster and stabilized GAN training for high-fidelity few-shot image synthesis. In *International Conference on Learning Representations*, 2021.
- Xingchao Liu, Chengyue Gong, and Qiang Liu. Flow straight and fast: Learning to generate and transfer data with rectified flow. *arXiv preprint arXiv:2209.03003*, 2022a.
- Zhuang Liu, Hanzi Mao, Chao-Yuan Wu, Christoph Feichtenhofer, Trevor Darrell, and Saining Xie. A ConvNet for the 2020s. In *Conference on Computer Vision and Pattern Recognition*, 2022b.
- Mario Lucic, Karol Kurach, Marcin Michalski, Sylvain Gelly, and Olivier Bousquet. Are GANs created equal? a large-scale study. In *Advances in Neural Information Processing Systems*, 2018.
- Muhammad Ferjad Naeem, Seong Joon Oh, Youngjung Uh, Yunjey Choi, and Jaejun Yoo. Reliable fidelity and diversity metrics for generative models. In *International Conference on Machine Learning*, 2020.
- Tim Salimans and Jonathan Ho. Progressive distillation for fast sampling of diffusion models. In *International Conference on Learning Representations*, 2022.
- Tim Salimans, Ian Goodfellow, Wojciech Zaremba, Vicki Cheung, Alec Radford, and Xi Chen. Improved techniques for training GANs. In *Advances in Neural Information Processing Systems*, 2016.
- Axel Sauer, Katja Schwarz, and Andreas Geiger. StyleGAN-XL: Scaling StyleGAN to large diverse datasets. In *ACM SIGGRAPH 2022 Conference Proceedings*, 2022.
- Vikash Sehwal, Caner Hazirbas, Albert Gordo, Firat Ozgenel, and Cristian Canton Ferrer. Generating high fidelity data from low-density regions using diffusion models. In *IEEE/CVF Conference on Computer Vision and Pattern Recognition*, 2022.
- Yang Song, Prafulla Dhariwal, Mark Chen, and Ilya Sutskever. Consistency models. In *International Conference on Machine Learning*, 2023.
- Jiayan Teng, Wendi Zheng, Ming Ding, Wenyi Hong, Jianqiao Wangni, Zhuoyi Yang, and Jie Tang. Relay diffusion: Unifying diffusion process across resolutions for image synthesis. In *International Conference on Learning Representations*, 2024.
- Ilya Tolstikhin, Neil Houlsby, Alexander Kolesnikov, Lucas Beyer, Xiaohua Zhai, Thomas Unterthiner, Jessica Yung, Andreas Steiner, Daniel Keysers, Jakob Uszkoreit, Mario Lucic, and Alexey Dosovitskiy. MLP-Mixer: An all-MLP architecture for vision. In *Advances in Neural Information Processing Systems*, 2021.

- Alexander Tong, Kilian Fatras, Nikolay Malkin, Guillaume Hugué, Yanlei Zhang, Jarrid Rector-Brooks, Guy Wolf, and Yoshua Bengio. Improving and generalizing flow-based generative models with minibatch optimal transport. *Transactions on Machine Learning Research*, 2024.
- Arash Vahdat and Jan Kautz. NVAE: A deep hierarchical variational autoencoder. In *Advances in Neural Information Processing Systems*, 2020.
- Arash Vahdat, Karsten Kreis, and Jan Kautz. Score-based generative modeling in latent space. In *Advances in Neural Information Processing Systems*, 2021.
- Chirag Vashist, Shichong Peng, and Ke Li. Rejection sampling IMLE: Designing priors for better few-shot image synthesis. In *European Conference on Computer Vision*, 2024.
- Guan Wang, Jin Li, Yuhao Sun, Xing Chen, Changling Liu, Yue Wu, Meng Lu, Sen Song, and Yasin Abbasi Yadkori. Hierarchical reasoning model. *arXiv preprint arXiv:2506.21734*, 2025.
- Zhisheng Xiao, Karsten Kreis, Jan Kautz, and Arash Vahdat. VAEBM: A symbiosis between variational autoencoders and energy-based models. In *International Conference on Learning Representations*, 2021.
- Zhisheng Xiao, Karsten Kreis, and Arash Vahdat. Tackling the generative learning trilemma with denoising diffusion GANs. In *International Conference on Learning Representations*, 2022.
- Tianwei Yin, Michaël Gharbi, Richard Zhang, Eli Shechtman, Frédo Durand, William T. Freeman, and Taesung Park. One-step diffusion with distribution matching distillation. In *IEEE/CVF Conference on Computer Vision and Pattern Recognition*, 2024.
- Bowen Zhang, Shuyang Gu, Bo Zhang, Jianmin Bao, Dong Chen, Fang Wen, Yong Wang, and Baining Guo. StyleSwin: Transformer-Based GAN for High-Resolution image generation. In *IEEE/CVF Conference on Computer Vision and Pattern Recognition*, 2022.
- Richard Zhang, Phillip Isola, Alexei A Efros, Eli Shechtman, and Oliver Wang. The unreasonable effectiveness of deep features as a perceptual metric. In *Conference on Computer Vision and Pattern Recognition*, 2018.
- Linqi Zhou, Stefano Ermon, and Jiaming Song. Inductive moment matching. *arXiv preprint arXiv:2503.07565*, 2025.

A Recursive Token Mapper: algorithmic description

Algorithm 1 gives the full forward pass of RTM, including the short-gradient optimization. A single IMLE loss is computed on the final style w ; no supervision is applied at intermediate steps.

Algorithm 1 Recursive Token Mapper (RTM): Noise to Style

Require: Noise vector $z \in \mathbb{R}^d$, refinement steps H , inner cycles L
Ensure: Style vector $w \in \mathbb{R}^d$

- 1: $Z_0 \leftarrow \text{Reshape}(W_{\text{proj}} \cdot z + b_{\text{proj}}) \in \mathbb{R}^{s \times d_h}$ // Project noise to tokens
- 2: $Z_H \leftarrow Z_H^{\text{init}}, Z_L \leftarrow Z_L^{\text{init}}$ // Initialize carry from fixed vectors
- 3: **for** $h = 1$ **to** H **do**
- 4: **for** $\ell = 1$ **to** L **do**
- 5: $Z_L \leftarrow f(Z_L, Z_H + Z_0)$ // L-level update with noise re-injection
- 6: **end for**
- 7: $Z_H \leftarrow f(Z_H, Z_L)$ // H-level update
- 8: **if** $h < H$ **then**
- 9: $Z_H \leftarrow \text{detach}(Z_H), Z_L \leftarrow \text{detach}(Z_L)$ // Short-gradient: detach after non-final step
- 10: **end if**
- 11: **end for**
- 12: $w \leftarrow W_{\text{out}} \cdot \text{Flatten}(Z_H) + b_{\text{out}}$ // Readout to style vector
- 13: **return** w // Loss is computed on w only

B Theoretical analysis

We make two short observations that justify replacing the StyleGAN MLP mapper with RTM. First, RTM keeps the IMLE coverage guarantee that motivates the loss. Second, RTM’s compute budget is set by the inference-time schedule, not by its parameter count.

Throughout, write the generator as $T_\theta = G_\phi \circ M_\psi$, with mapper $M_\psi : \mathcal{Z} \rightarrow \mathcal{W}$ and decoder $G_\phi : \mathcal{W} \rightarrow \mathcal{X}$. Given training data $\{x_i\}_{i=1}^n$, a distance d , and a latent prior p , IMLE [Li and Malik, 2018, Vashist et al., 2024] draws m candidate latents $z_1, \dots, z_m \sim p$ and minimizes

$$\mathcal{L}_{\text{IMLE}}(\theta) = \mathbb{E}_{z_{1:m}} \left[\sum_{i=1}^n \min_{j \in [m]} d(x_i, T_\theta(z_j)) \right]. \quad (2)$$

Lemma 1 (Coverage is preserved). *Fix the decoder G_ϕ , a training point x , and a tolerance $\varepsilon > 0$. Assume there is some style w^* with $d(x, G_\phi(w^*)) \leq \varepsilon/2$ and that G_ϕ is locally Lipschitz at w^* . Then for any continuous mapper M_ψ that maps some latent z^* with $p(z^*) > 0$ close to w^* , the probability that none of m candidate latents lands within ε of x vanishes as $m \rightarrow \infty$.*

Proof. Local Lipschitz-ness of G_ϕ at w^* gives a $\delta > 0$ such that $\|w - w^*\| \leq \delta$ implies $d(G_\phi(w), G_\phi(w^*)) \leq \varepsilon/2$. Continuity of M_ψ at z^* then provides a neighbourhood U of z^* that M_ψ sends into $B(w^*, \delta)$. Because $p(z^*) > 0$, we have $\Pr[z \in U] = q > 0$, so the chance that none of the m candidates lands in U is at most $(1 - q)^m \rightarrow 0$. On the complementary event, the triangle inequality gives $d(x, T_\theta(z_j)) \leq \varepsilon$ for that candidate. \square

A standard MLP mapper and an RTM are both continuous compositions of differentiable layers, so the lemma applies to both: swapping in an RTM does not weaken the coverage guarantee. The same argument carries over to RS-IMLE [Vashist et al., 2024], which only changes the prior p via rejection sampling and so preserves both positive density and continuity.

The second point is purely structural. The trainable parameters of an RTM are the projection, the readout, the shared block, and (when learnable) the carry initializations. None of these scales with the schedule (H, L) . From Algorithm 1, the shared block is evaluated $H \cdot (L + 1)$ times per sample. So compute can be turned up or down at inference time without changing the parameter count, which is what makes RTM parameter-efficient.

C Decoder architectures

The mapping network is the only component we change; the convolutional decoder is shared with each baseline. Figure 4 shows the per-dataset decoder pipelines used in our RS-IMLE experiments, and the table beneath the diagrams gives their key hyper-parameters. Each pipeline starts from a constant feature map at 1×1 , progressively upsamples through a stack of residual blocks, and emits an RGB image through a final 1×1 convolution. The CIFAR-10 and CelebA-HQ runs use the same ConvNeXt-style residual blocks [Liu et al., 2022b]; the few-shot runs use the standard $1 \times 1/3 \times 3$ residual blocks with GELU activations from adapted RS-IMLE [Vashist et al., 2024] codebase. The style code w from the mapper modulates every block via Adaptive Instance Normalization [Huang and Belongie, 2017], and spatial noise injection is applied at resolutions ≤ 256 .

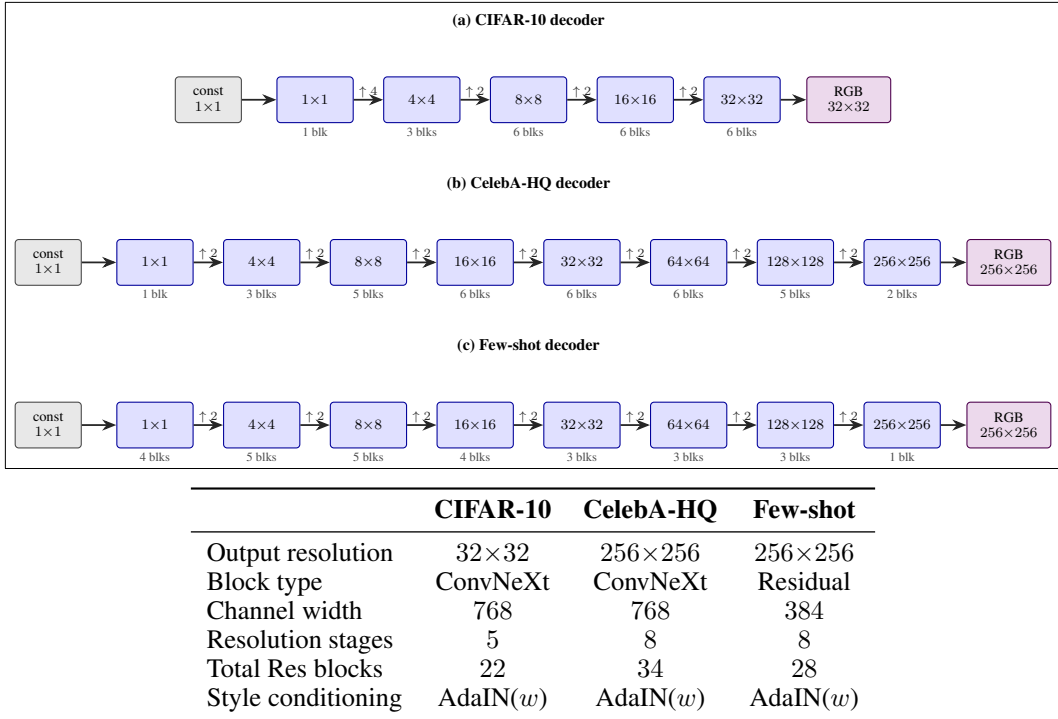


Figure 4: Decoder architectures used across our RS-IMLE experiments.

D Few-shot image generation

We evaluate RTM on the nine standard few-shot image-generation benchmarks used by Vashist et al. [2024]. Each benchmark contains only a few hundred training images to test RTM under limited data.

Setup. We use the nine standard few-shot benchmarks used by RS-IMLE Vashist et al. [2024] (Obama, Grumpy Cat, Panda, FFHQ-100, Cat, Dog, Anime, Skulls, Shells), each containing 64–389 training images at 256×256 . All RS-IMLE runs share the same decoder, optimiser, and rejection-sampling threshold; the only thing that changes between the matched RS-IMLE baseline and the RTM rows is the mapping network. RTM uses a single configuration $(H, L)=(8, 2)$ shared across all nine datasets, with no per-dataset tuning. We compare against FastGAN [Liu et al., 2021], AdaIMLE [Aghabozorgi et al., 2023], the published RS-IMLE numbers [Vashist et al., 2024], and our own controlled reproduction of RS-IMLE that uses an identical pipeline to the RTM runs. The rightmost column of Table 5 ablates the original TRM attention block in place of MLP-Mixer for the shared block f .

Results. RTM with the MLP-Mixer block roughly halves the average FID of the matched RS-IMLE reproduction. Because the only thing that changes between the two rows is the mapping network, this

Table 5: FID on nine few-shot benchmarks (256×256 , 5,000 samples). **Bold**: best per row.

Dataset	FastGAN	AdaIMLE	RS-IMLE (Paper)	RS-IMLE (Reprod.)	Ours (MLP Mix)	Ours (Attention)
Obama	41.1	25.0	14.0	17.3	10.19	12.05
Grumpy Cat	26.6	19.1	11.5	13.1	6.70	11.53
Panda	10.0	7.6	3.5	8.0	6.73	4.70
FFHQ-100	54.2	33.2	12.9	19.8	13.23	13.68
Cat	35.1	24.9	15.9	17.5	8.62	14.44
Dog	50.7	43.0	23.1	47.0	16.09	19.44
Anime	69.8	65.8	35.8	24.8	18.04	17.21
Skulls	109.6	81.9	51.1	42.4	21.36	43.01
Shells	120.9	108.5	55.4	37.15	24.48	26.37
Average	57.6	45.4	24.8	25.2	13.94	18.05

improvement is attributable to the mapper’s recursive structure rather than to capacity, optimizer, or training schedule. The published RS-IMLE numbers retain a small edge on a couple of individual datasets, but our controlled reproduction sits well above those numbers, suggesting that part of the published gap reflects per-dataset tuning that we did not attempt; against the matched reproduction, RTM wins on average and on the majority of benchmarks.

Choice of block. The attention-based RTM ablation in the rightmost column tracks the MLP-Mixer variant within a few FID points on most datasets but is worse on average (18.05 vs. 13.94) and is consistently slower per training step because of the quadratic cost of self-attention on the sequence of tokens. The MLP-Mixer block is therefore used for all of the larger CIFAR-10, CelebA-HQ, AFHQ-v1, and StyleGAN runs in the main paper. Qualitative samples for a selection of few-shot datasets are shown in Figures 5–8; per-dataset Precision and Recall numbers are reported in Section E.

E Per-dataset Precision and Recall on few-shot benchmarks

Table 6 gives Precision and Recall per dataset for all few-shot benchmarks. Both RTM variants match or exceed the baselines in precision, and the attention variant delivers the second-highest average recall (0.88), only slightly below the strong RS-IMLE reproduction baseline (0.94), but with substantially lower FID (Table 5). The recall drop on datasets like Skulls and Shells is expected: with only a few dozen training images, the dataset itself is too small for recall to be a meaningful metric. On larger, more varied datasets such as Dog, RTM maintains strong Recall while improving Precision.

F Implementation details and training stability

Optimization. All RS-IMLE runs use Adam with $\beta_1 = 0.5$, $\beta_2 = 0.999$. All dataset-specific hyperparameters, including learning rate, batch size, training schedule, and RTM configuration (H , L), are provided in the configuration files released with the code.

Short-gradient Optimization. As described in Section 3.2, only the final refinement step is differentiated through; all preceding steps are detached. This is the dominant memory saving in RTM, and is what allows us to train deep configurations ($H=8$, $L=2$ etc.) on a single GPU.

Compute. All experiments were run on NVIDIA H100 GPUs. RS-IMLE runs (baseline and RTM) on CIFAR-10 take approximately two weeks on 4 H100 GPUs; on CelebA-HQ at 256×256 they take approximately three weeks on 4 H100 GPUs. Few-shot runs (baseline and RTM) take approximately 16 hours on a single H100 GPU for the smaller benchmarks (Shells, Skulls) and up to 2 days for the larger ones (Dog). StyleGAN2 runs (baseline and RTM) on CIFAR-10 take approximately 24 hours on a single H100 GPU. StyleGAN2-ADA runs (baseline and RTM) on CIFAR-10 take approximately

Table 6: Precision and Recall on the nine few-shot benchmarks (256×256 , 1,000 samples). **Bold:** best per metric.

Dataset		FastGAN	AdaIMLE	RS-IMLE (Paper)	RS-IMLE (Reprod.)	Ours (MLP Mix)	Ours (Attention)
Obama	Prec.	0.92	0.99	0.98	0.99	1.00	1.00
	Rec.	0.09	0.68	0.82	0.97	0.64	0.83
Grumpy Cat	Prec.	0.91	0.97	0.93	0.99	1.00	0.99
	Rec.	0.13	0.72	0.95	0.97	0.65	0.94
Panda	Prec.	0.96	0.98	0.99	0.99	0.99	1.00
	Rec.	0.16	0.63	0.97	0.84	0.93	0.90
FFHQ-100	Prec.	0.91	0.99	1.00	1.00	1.00	1.00
	Rec.	0.13	0.77	0.99	0.99	0.65	0.89
Cat	Prec.	0.97	0.98	0.96	0.97	1.00	0.98
	Rec.	0.08	0.86	0.98	0.99	0.80	0.98
Dog	Prec.	0.96	0.97	0.98	0.97	0.99	0.99
	Rec.	0.19	0.61	0.94	0.76	0.92	0.89
Anime	Prec.	0.86	0.92	0.95	0.97	0.99	0.98
	Rec.	0.08	0.59	0.91	1.00	0.75	0.96
Skulls	Prec.	0.78	0.95	0.99	0.98	0.99	0.99
	Rec.	0.03	0.32	0.65	0.98	0.63	0.68
Shells	Prec.	0.92	0.97	0.98	0.99	0.99	1.00
	Rec.	0.03	0.62	0.59	0.97	0.66	0.81
Average	Prec.	0.91	0.97	0.97	0.98	0.99	0.99
	Rec.	0.10	0.64	0.87	0.94	0.74	0.88

4 days on a single H100 GPU. StyleGAN2-ADA runs (baseline and RTM) on AFHQ-v1 at 512×512 take approximately 4 days on 4 H100 GPUs.

Dataset Licenses. CIFAR-10 is freely available for research and commercial use; we cite the original technical report [Krizhevsky, 2009]. CelebA-HQ [Karras et al., 2018] is restricted to non-commercial research and educational use. AFHQ-v1 [Choi et al., 2020] is released under the Creative Commons Attribution-NonCommercial 4.0 International (CC BY-NC 4.0) license. The StyleGAN2 and StyleGAN2-ADA codebases [Karras et al., 2020b,a] are released under the NVIDIA Source Code License. We use all datasets and codebases strictly for non-commercial research purposes

G StyleGAN Evaluation Protocol

Table 3 uses the StudioGAN evaluation pipeline of Kang et al. [2021], which implements Improved Precision/Recall [Kynkäänniemi et al., 2019] and Density/Coverage [Naeem et al., 2020]. The CIFAR-10 “StyleGAN2 (no RTM)” row reports the best-FID checkpoint of the StudioGAN baseline at 170,000 steps. The FID and Precision/Recall implementations used in this pipeline differ slightly in feature extractor, reference statistics, and image preprocessing from those used in Tables 1 and 2.

H Inference Latency

Inference latency is measured as the amortized wall-clock time per generated image on a single NVIDIA H100 GPU. We synchronize the device, time one complete forward pass of the full generator (EMA weights, no gradient) over a batch of noise vectors, and divide the elapsed time by the batch size. We use batch size 64 for CIFAR-10 and batch size 16 for CelebA-HQ at 256×256 , reflecting memory constraints at the higher resolution. Each reported value is the median batch time over 200 forward passes, preceded by 20 warm-up passes to stabilize GPU cache state.

I Depth-only Ablation: a deeper non-recursive MLP mapper

Our main StyleGAN2 results in Table 3 replace a 2-layer MLP mapping network with an RTM that applies the shared block $H \cdot (L + 1) = 16 \cdot 2 = 32$ times per forward pass (Appendix B). To check whether the gain comes from depth (more sequential transformations of z) rather than from recursion (the same parameters reused across cycles), we train two additional StyleGAN2 variants that swap the 2-layer MLP for a non-recursive 16- or 32-layer MLP and are otherwise identical to the StudioGAN baseline. The 32-layer MLP is the true depth-matched baseline: it applies the same number of sequential transformations as RTM.

Table 7: Depth-only ablation on CIFAR-10 with StyleGAN2: only the mapping network changes. The RTM config $(H, L)=(16, 1)$ applies the shared block $H \cdot (L+1) = 32$ times per forward pass, so the 32-layer MLP is the depth-matched non-recursive baseline. **Bold**: best per metric.

Mapping network	Mapper params	FID ↓	IS ↑	Prec. ↑	Rec. ↑
2-layer MLP (StudioGAN baseline)	0.53M	3.88	10.20	0.734	0.664
16-layer MLP (half-depth, non-recursive)	4.2M	3.73	10.18	0.751	0.616
32-layer MLP (depth-matched, non-recursive)	8.4M	4.32	10.51	0.769	0.550
RTM, $(H, L)=(16, 1)$ (Ours)	0.66M	3.55	10.21	0.740	0.661

Setup. Each MLP variant takes the same StyleGAN2 backbone as the StudioGAN baseline and only deepens the mapping network from 2 to 16 or 32 layers; everything else (decoder, discriminator, optimizer, training schedule) is unchanged. All rows are trained for the same 200,000 steps on the same CIFAR-10 split, and we report the best-FID checkpoint of each run. RTM uses the MLP-Mixer block with $(H, L) = (16, 1)$; per the formula in Appendix B, this gives $H \cdot (L+1) = 32$ shared-block evaluations per forward pass, matching the sequential depth of the 32-layer MLP.

Observation. Increasing non-recursive depth from 2 to 16 layers improves FID (3.73 vs. 3.88), confirming that the mapping network is sensitive to sequential depth. Further deepening to 32 layers reverses this trend (4.32 FID), suggesting that very deep non-recursive MLPs overfit the mapping task without the regularising effect of parameter sharing. The 32-layer MLP achieves the highest Precision (0.769) and IS (10.51), but at a severe cost to Recall (0.550 vs. 0.664 for the 2-layer baseline), consistent with a high-capacity non-recursive mapper that concentrates probability mass on the high-density modes of the data distribution. RTM achieves the best FID (3.55) with $13\times$ fewer parameters than the depth-matched MLP (0.66M vs. 8.4M), and maintains Recall close to the 2-layer baseline (0.661 vs. 0.664). The recursive structure thus provides a more effective inductive bias than raw depth: parameter sharing across cycles improves distributional fidelity without sacrificing coverage.

J Qualitative few-shot samples

Figures 5–8 show random samples from our MLP token-mixing RTM on four few-shot benchmarks. Figures 9 and 10 show SLERP interpolations in latent space for the same four benchmarks.



Figure 5: Random samples from RS-IMLE + RTM on Shells.



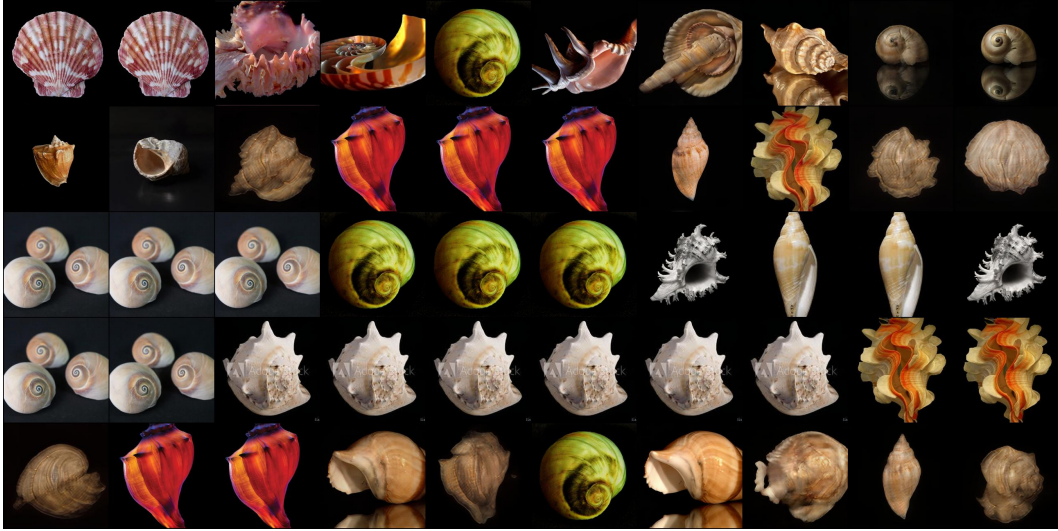
Figure 6: Random samples from RS-IMLE + RTM on Dog.



Figure 7: Random samples from RS-IMLE + RTM on Cat.



Figure 8: Random samples from RS-IMLE + RTM on Anime.



(a) Shells



(b) Dog

Figure 9: SLERP interpolations in latent space from RS-IMLE + RTM on Shells and Dog.



(a) Cat



(b) Anime

Figure 10: SLERP interpolations in latent space from RS-IMLE + RTM on Cat and Anime.

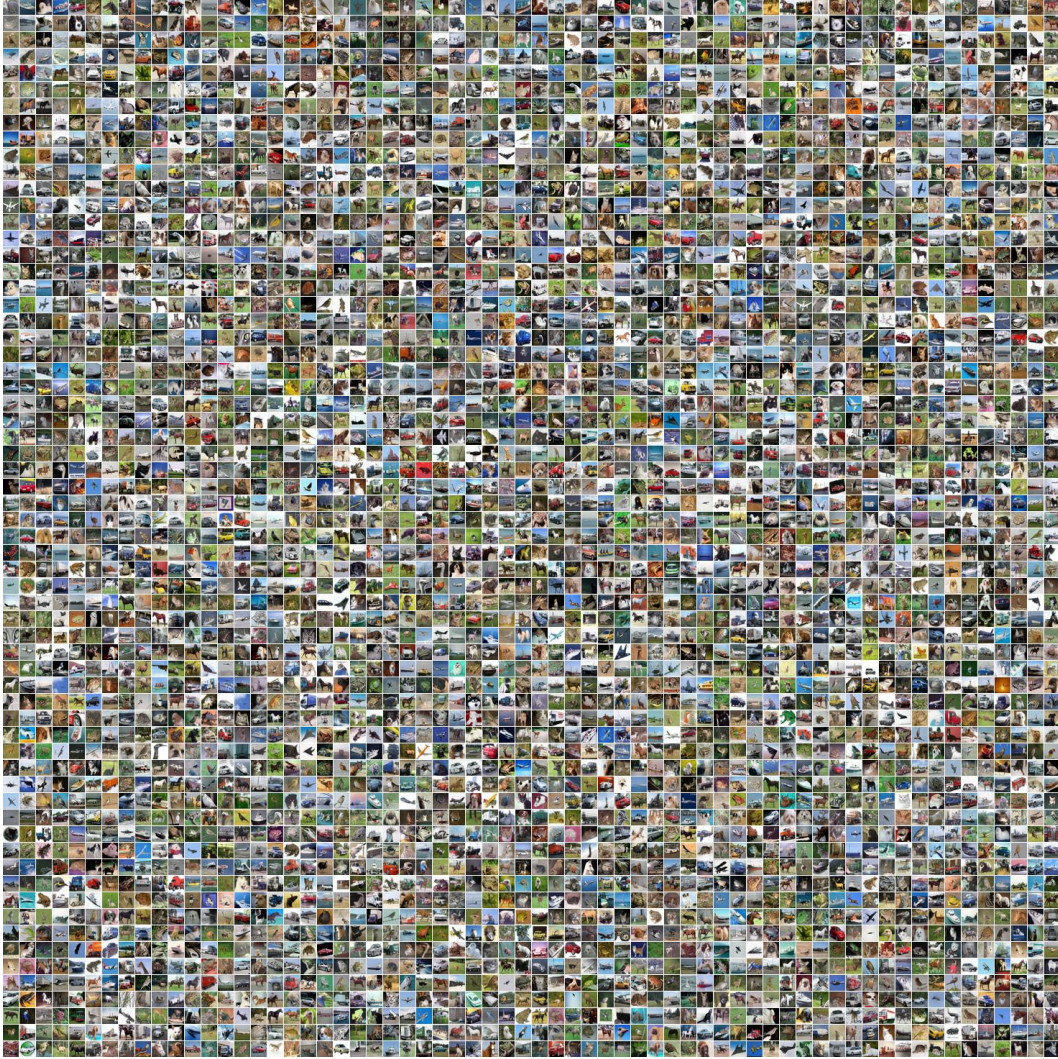


Figure 11: $\sim 4,000$ unconditional CIFAR-10 samples from our RS-IMLE + RTM, ($H=16, L=1$). Best viewed zoomed in.

K Qualitative CIFAR-10 samples

Figure 11 shows $\sim 4,000$ random samples from our ($H=16, L=1$) RTM on CIFAR-10. At this density, every CIFAR-10 class is represented hundreds of times and within-class appearance varies in colour, pose, scale, and background, consistent with the high Recall reported in Table 1.

L Baseline-vs-RTM qualitative comparisons

Every block in Figures 12 and 13 is anchored on a single query image taken from the real dataset and paired with the nearest neighbours from each model’s generated pool in Inception feature space. The top row shows neighbours from the RS-IMLE baseline, and the bottom row shows neighbours from RS-IMLE + RTM. The model whose neighbours more faithfully reproduce the query is the better matcher.



Figure 12: RS-IMLE+RTM neighbours more faithfully match the query across gender, skin tone, age, and hair attributes that the baseline often fails to preserve.

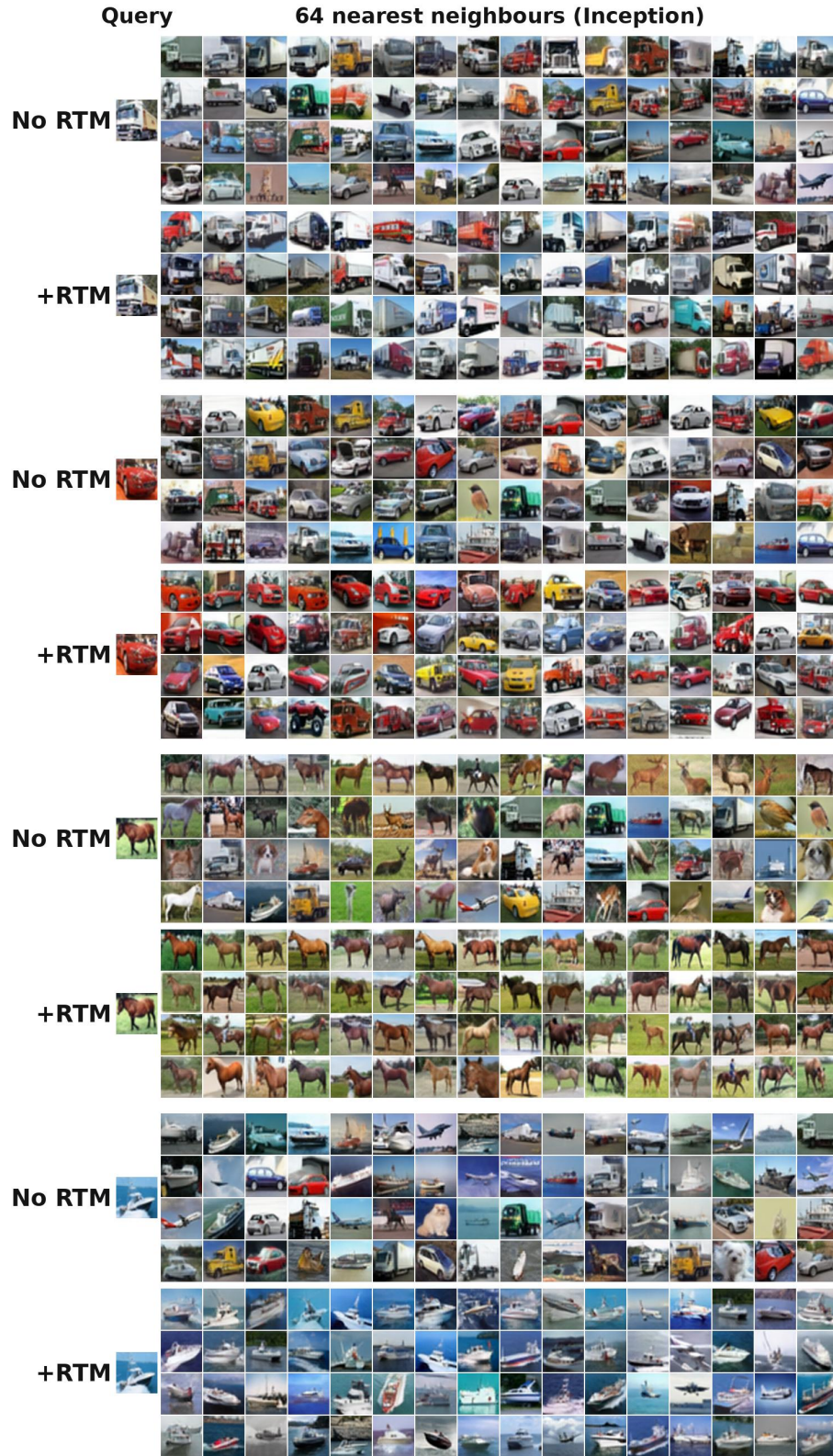


Figure 13: RS-IMLE+RTM neighbours better cluster around the query’s class and visual characteristics, reflecting improved mode coverage over the baseline.



Figure 14: CelebA-HQ 256×256 comparison between RS-IMLE baseline and RS-IMLE + RTM. Top: left is without RTM, right is with RTM. Bottom: top rows are without RTM, bottom rows are with RTM. RTM generates sharper images with greater variety in age, skin tone, and expression, consistent with the improved Precision and Recall in Table 2.

M CelebA-HQ baseline vs. RTM

Figure 14 compares RS-IMLE and RS-IMLE + RTM on CelebA-HQ at 256×256 . The top panel shows matched sample pairs. The bottom panel shows a broader set of generations from each model, illustrating the gain in both sample quality and diversity consistent with the Precision and Recall improvements in Table 2.

N Additional samples

Figures 15–16 show unconditional CelebA-HQ 256×256 samples from RS-IMLE + RTM. Figures 17 and 18 show additional baseline-vs-RTM AFHQ-v1 comparisons for the StyleGAN2-ADA setup.

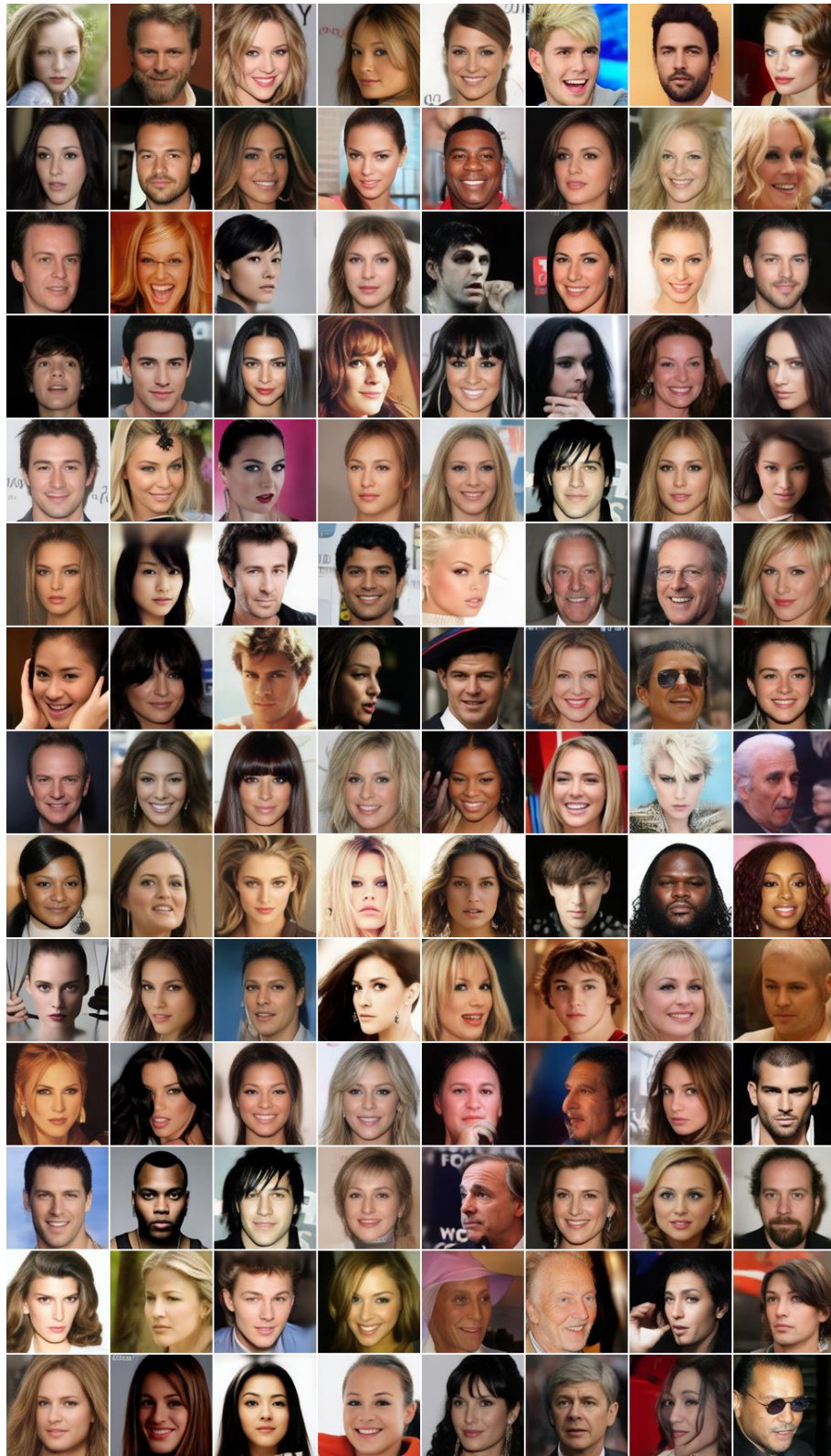


Figure 15: Unconditional CelebA-HQ 256×256 samples from RS-IMLE + RTM.

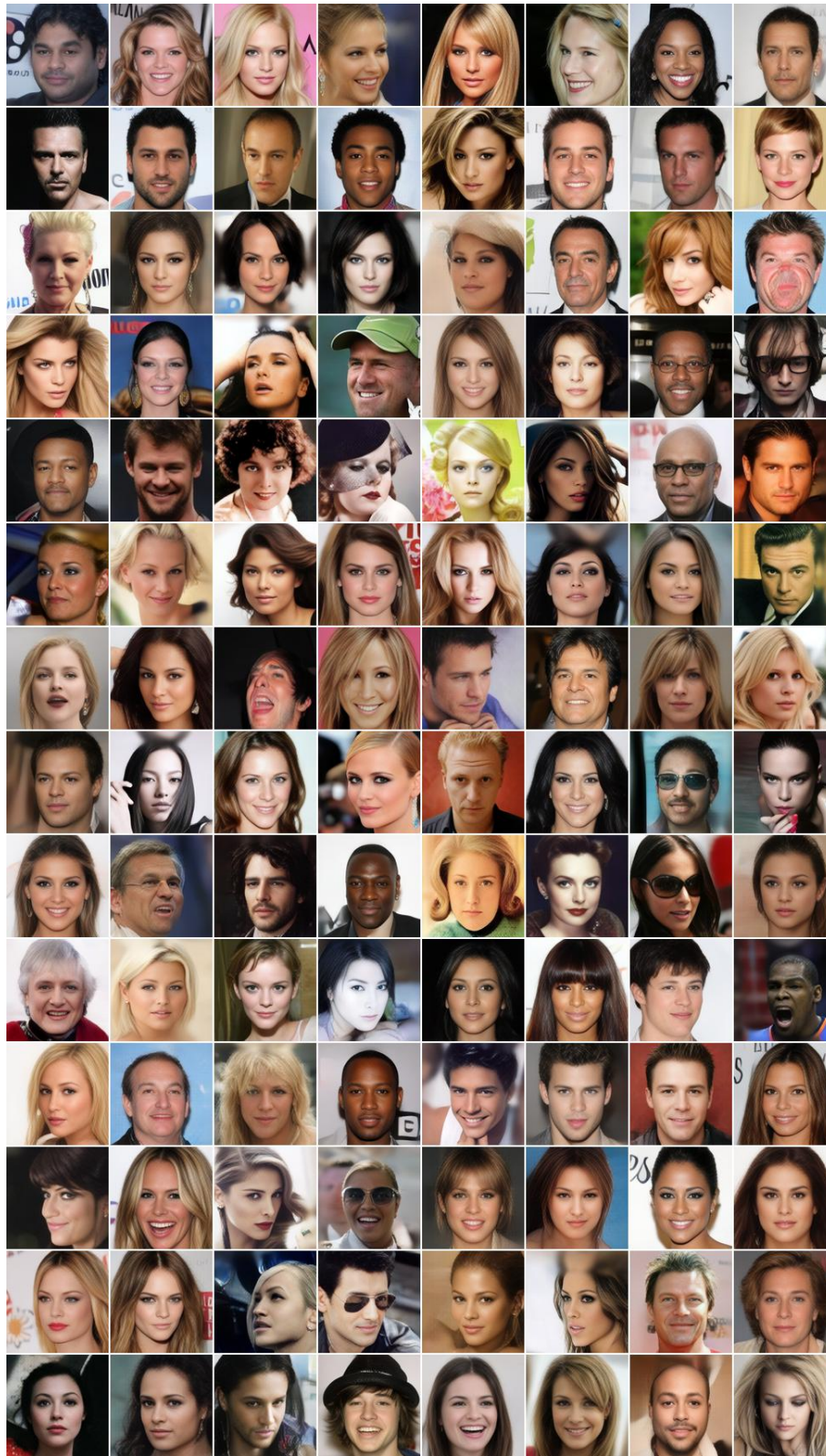


Figure 16: Unconditional CelebA-HQ 256×256 samples from RS-IMLE + RTM.



Figure 17: AFHQ-v1 with StyleGAN2-ADA. Top: baseline. Bottom: with our RTM mapper. First set of examples.



Figure 18: AFHQ-v1 with StyleGAN2-ADA. Top: baseline. Bottom: with our RTM mapper. Second set of examples.